Electromagnon with Sensitive Terahertz Magnetochromism in a Room-Temperature Magnetoelectric Hexaferrite

Sae Hwan Chun,[1] Kwang Woo Shin,[1] Hyung Joon Kim,[1] Seonghoon Jung,[2] Jaehun Park,[2] Young-Mi Bahk,[3] Hyeong-Ryeol Park,[3] Jisoo Kyoung,[3] Da-Hye Choi,[4] Dai-Sik Kim,[3] Gun-Sik Park,[4] J. F. Mitchell,[5] and Kee Hoon Kim[1,*]

[1]*CeNSCMR, Department of Physics and Astronomy, Seoul National University, Seoul 08826, South Korea*
[2]*Pohang Accelerator Laboratory, Pohang, Gyeongbuk 37673, South Korea*
[3]*Nano Optics Group, Department of Physics and Astronomy, Seoul National University, Seoul 08826, South Korea*
[4]*Center for THz-driven Biomedical Systems, Department of Physics and Astronomy, Seoul National University, Seoul 08826, South Korea*
[5]*Materials Science Division, Argonne National Laboratory, Argonne, Illinois 60540, USA*

(Received 26 February 2017; published 12 January 2018)

An electromagnon in the magnetoelectric (ME) hexaferrite $Ba_{0.5}Sr_{2.5}Co_2Fe_{24}O_{41}$ (Co_2Z-type) single crystal is identified by time-domain terahertz (THz) spectroscopy. The associated THz resonance is active on the electric field (E^{ω}) of the THz light parallel to the c axis ($\parallel$ [001]), whose spectral weight develops at a markedly high temperature, coinciding with a transverse conical magnetic order below 410 K. The resonance frequency of 1.03 THz at 20 K changes -8.7% and $+5.8\%$ under external magnetic field (H) of 2 kOe along [001] and [120], respectively. A model Hamiltonian describing the conical magnetic order elucidates that the dynamical ME effect arises from antiphase motion of spins which are coupled with modulating electric dipoles through the exchange striction mechanism. Moreover, the calculated frequency shift points to the key role of the Dzyaloshinskii-Moriya interaction that is altered by static electric polarization change under different H.

DOI: 10.1103/PhysRevLett.120.027202

Quasiparticles in condensed matter manifest their collective interactions that lead to emergent phenomena and entanglement among various degrees of freedom. An electromagnon, the magnetic excitation induced by electric-dipole activeness, is one example representing entangled magnetic and electric properties in the dynamical regime [1,2]. It is generally observed as a magnon driven by the photoinduced oscillation of electric polarization (P) and can be found in multiferroics [3–9] that manifest the static magnetoelectric (ME) effect, i.e., cross control of electric polarization and magnetization by magnetic and electric fields [10–13]. This dynamical ME effect is expected to mirror the character of the ME ground state that shares the same ME coupling origins [2,4,14–16]: inverse Dzyaloshinskii-Moriya (DM) interaction [17], exchange striction [18], and spin-dependent covalency between ligand p state and metal d state (p-d hybridization) [19]. An intriguing aspect of the ME state, however, is that the dynamics do not always correspond with the static ground state. For example, $R\mathrm{MnO_3}$ (R = rare earth ion) [3,20–22] and $Ba_2Mg_2Fe_{12}O_{22}$ (Mg_2Y-type hexaferrite) [5] display the dynamical ME effect associated with the exchange striction, while the static effect is induced by the inverse DM interaction. $Cu(Fe, Ga)O_2$ separately hosts dynamical and static effects in different magnetic phases despite the same ME coupling origin of the p-d hybridization [6]. These peculiar characteristics of the ME phenomena calls for deeper understanding of the underlying physics.

Beyond this scientific perspective, an electromagnon residing in the terahertz (THz) frequency range points to the potential of application in the THz technology [23]. This emerging technology aims to exploit the broadband of THz light suitable for fast mass data-transfer communication devices, or enhanced sensitivity to water molecules applicable for biomedical sensing. In multiferroics, the capability to control the THz resonance profile associated with an electromagnon by external magnetic field (H) [3–9] is thought of as a key attribute for realizing a novel application such as H-controlled THz filtering devices. This objective, however, is challenged in most multiferroics because of the low operation temperature needed for realizing the dynamical ME effect and high magnetic field for manipulating THz light.

Magnetoelectric hexaferrites are candidates that fulfill both scientific and technological aspirations. The electromagnon of the Mg_2Y-type hexaferrite demonstrates THz light absorption and the resonance frequency tunable by an external magnetic field [5]. This dynamical ME effect is associated with the noncollinear spins forming conical magnetic structures confirmed below 164 K. On the other hand, the Co_2Z-type hexaferrite, $(Ba, Sr)_3Co_2Fe_{24}O_{41}$ hosts a transverse conical magnetic order that persists up to the remarkably high temperature of $\sim$410 K for the Sr_3Co_2Z-type and $Ba_{0.5}Sr_{2.5}Co_2Z$-type hexaferrites. This magnetic state realizes the room-temperature static ME effects such as low-magnetic-field control of electric

polarization [24,25] and electric-field control of magnetization [26]. The dynamical ME effect is expected to also exist, but identification of the electromagnon has been hindered by the lack of a single crystal with the proper size for the investigation despite the recent discovery of magnons in the Co_2Z-type ceramics [27].

In this Letter, we report the presence of the electromagnon in $Ba_{0.5}Sr_{2.5}Co_2Fe_{24}O_{41}$ from the THz time-domain spectroscopy. Study of the single crystals allows us to unambiguously evidence the electric-dipole activeness and observe sensitive shifts of the THz resonance frequencies according to external magnetic field directions. We establish a model Hamiltonian that successfully identifies a magnon mode corresponding to the electromagnon. The model calculation of the magnon mode also reveals that the field-direction dependent frequency shifts can be properly explained by consideration of the DM interaction associated with the static ME effect in the Hamiltonian. This interconnection between the dynamical and static ME effects may offer a novel route to enhance the THz-device functionality.

Single crystals of $Ba_{0.5}Sr_{2.5}Co_2Fe_{24}O_{41}$ (5 mm × 5 mm × 3 mm) were grown by a flux method [26] and were thinned down to 100–350 μm for THz time-domain spectroscopy (THz TDS) that employed a 1 mm-focused beam with the transmission geometry. The THz-light resonance arising from the electromagnon was identified from the absorption profiles obtained in various polarization of the light. The temperature dependence of data was obtained with a closed-cycle optical cryostat at the fs-THz beam line of the Pohang Accelerator Laboratory and the data above room temperature were verified using an independent THz TDS apparatus at Seoul National University. An external dc magnetic field of 2 kOe was applied to the samples with the Voigt geometry [5] by placing neodymium magnets near the samples. The field monitored by a Hall sensor did not change significantly in the temperature window of our interest.

$Ba_{0.5}Sr_{2.5}Co_2Fe_{24}O_{41}$ has a layered structure of hexagonal lattice (close to the space group $P6_3/mmc$) that has various channels of superexchange along the layers [Fig. 1(a)]. The layers can be grouped into magnetic building blocks labeled as L and S according to the dominant superexchange in each block, within which nearly antiparallel spin alignment is formed [25]. Thus, magnetic structures are effectively represented by composition of the net magnetic moments in the L and S blocks, $\vec{\mu}_L$ and $\vec{\mu}_S$. At the boundary of the blocks, a moderate superexchange in combination with single ion anisotropy yields diverse magnetic structures as temperature is varied. For instance, this Co_2Z-type hexaferrite undergoes the c axis-collinear ferrimagnetic order at 680 K with change of the easy axis close to the ab plane at 490 K, and then the transverse conical order at $T_{con} = \sim 410$ K [25,26].

Figures 2(a) and 2(b) show dielectric constants in THz range at 20 K converted from the absorption profile. To find

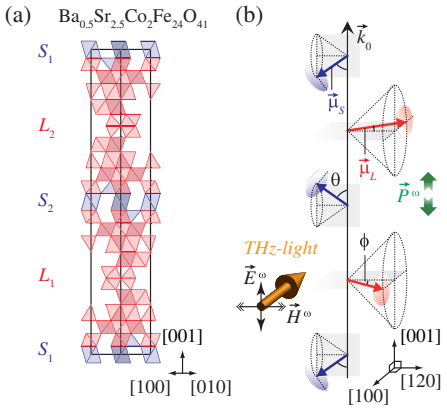

FIG. 1. (a) Crystal structure of $Ba_{0.5}Sr_{2.5}Co_2Fe_{24}O_{41}$ representing stacking of magnetic S (blue) and L (red) blocks. (b) Schematic illustration of transverse conical order (dotted lines) composed of $\vec{\mu}_S$ (blue arrow) and $\vec{\mu}_L$ (red arrow). Blue and red ellipsoids represent trajectories of the moment modulations. θ and ϕ refer to the angles of $\vec{\mu}_S$ from [001] and $\vec{\mu}_L$ from [120], respectively.

the resonance characteristic, i.e., an abrupt, steplike drop in the real part (ε_1) and sharp peak in the imaginary part (ε_2), we explored various configurations of the incident light polarization ($E^\omega \& H^\omega$) with respect to the crystallographic axes. Note that the configuration of $E^\omega \| [001] \& H^\omega \| [120]$ (denoted as $E^\omega_{[001]} H^\omega_{[120]}$) shows the most pronounced resonance features in the dielectric constants at 1.03 THz (≈4.26 meV). The resonance in this frequency regime may arise from magnetic excitations, including the putative electromagnon or alternatively conventional AFMR (antiferromagnetic resonance) excited by E^ω and

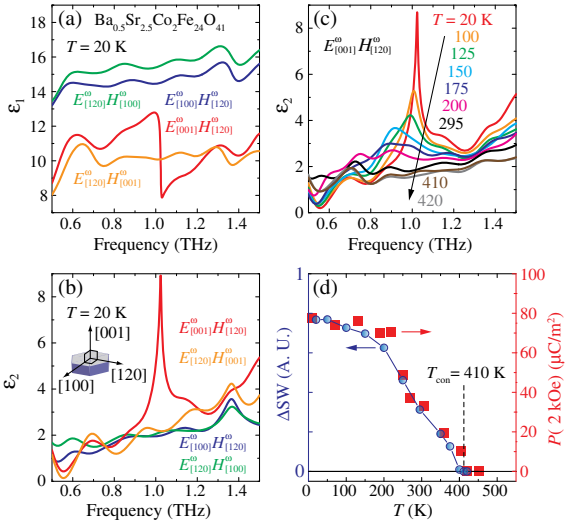

FIG. 2. Spectra of real (a) and imaginary (b) parts of complex dielectric constant for various E^ω & H^ω configurations at 20 K. (c) Temperature dependence of the ε_2 spectra for $E^\omega_{[001]} H^\omega_{[120]}$. (d) Temperature evolution of ΔSW (left axis) and the static $P \| [100]$ (right axis) in a single ME domain state at $H =$ 2 kOe$\|[120]$ (Ref. [26]). T_{con} refers to transition temperature of the transverse conical state.

H^{ω}, respectively. We find that the resonance does not occur in another configuration of the same H^{ω}, e.g. $E^{\omega}_{[100]}H^{\omega}_{[120]}$, which rules out AFMR as the origin [Fig. 2(a)]. The resonance was also observed in the configuration of the same E^{ω}, e.g. $E^{\omega}_{[001]}H^{\omega}_{[100]}$ (not shown). This establishes the electric-dipole activeness on $E^{\omega}\|[001]$ and conclusively proves the electromagnon in the Co_2Z-type hexaferrite. An alternative way of proving the electromagnon is to observe coupling between phonon and magnon branches via experimental probes as, e.g., inelastic neutron scattering. Renormalization of both branches, for example, can provide an important clue to understand the nature of the electromagnon and the dynamical ME effects further.

The presence of the electromagnon at 20 K in the transverse conical phase implies its correlation with the magnetic order. We monitored the temperature (T) evolution of the ε_2 spectra up to 420 K, above $T_{\rm con} = 410$ K, and found that the resonant peak became broader and weaker, and shifted to lower frequency while approaching $T_{\rm con}$ [Fig. 2(c)]. Despite the difficulty in resolving the peak above 200 K, considerable spectral weight (SW) is noted, which gradually converges to the one near $T_{\rm con}$. This T dependence can be better displayed via $\Delta SW(T) = SW(T) - SW(410\ \mathrm{K})$, where $SW(T) = \int \omega\varepsilon_0\varepsilon_2(\omega, T)d\omega$ in the range of 0.5–1.3 THz. We compare in Fig. 2(d) $\Delta SW(T)$ to the value of static P ($P_{\rm Static}$), which is estimated in a single ME-domain state of the transverse conical order [26]. Note that T evolution of both ΔSW and $P_{\rm static}$ matches very well: both show a rapid drop above 200 K and approach zero above $T_{\rm con}$. This evidences the correlation of the SW with the transverse conical order. It is noteworthy that the finite ΔSW associated with the magnetic order below $T_{\rm con}$ supports the presence of the electromagnon even at room temperature in the Co_2Z-type hexaferrite.

The electromagnon resonance developed in the transverse conical order can be manipulated by external magnetic fields. The response of the conical order depends on the field directions so that the Co_2Z-type hexaferrite exhibits magnetochromism, i.e., H-directional dependence of the resonance frequency. Figure 3(a) shows the ε_2 spectra at 20 K for $H = 2$ kOe $\|[120]$ and $\|[001]$, which display the resonances at 1.09 and 0.94 THz, corresponding to blue- and redshifting of 5.8% and 8.7% from 1.03 THz for $H = 0$, respectively. We observe persistent magnetochromism at least up to 200 K on top of the general tendency of electromagnon softening [Fig. 3(b)], while the damped resonance feature above 200 K makes it difficult to capture the frequency shifting within the experimental resolution. Such sensitive magnetochromism induced by application of relatively small H is a feature of the dynamical ME effect in the transverse conical state, offering an opportunity to realize new functional THz devices.

We now turn to elucidating the origin of the electromagnon resonance by assessing the relevant magnon mode. An effective Hamiltonian $\mathscr{H}$ is introduced on the basis of the L & S block model [28],

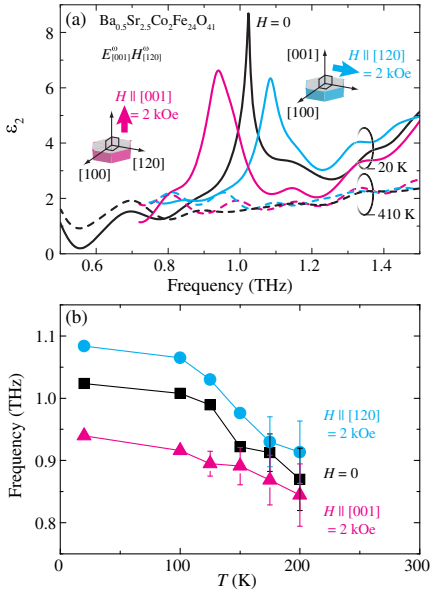

FIG. 3. ε_2 spectra for $E^{\omega}_{[001]}H^{\omega}_{[120]}$ under $H = 2$ kOe$\|[120]$ (blue), $\|[001]$ (red), and 0 kOe (black). Solid (dashed) curves correspond to the data at 20 K (410 K). Inset shows H directions applied to the sample. (b) Temperature dependence of the resonance frequencies upon the H directions.

$$\mathscr{H} = J_{LS}\sum_{i,j=1,2}(\vec{\mu}_{Si}\cdot\vec{\mu}_{Lj}) + 2J_{LL}(\vec{\mu}_{L1}\cdot\vec{\mu}_{L2}) + 2J_{SS}(\vec{\mu}_{S1}\cdot\vec{\mu}_{S2}) + D_L\sum_{i=1,2}(\mu_{Liz})^2 + D_S\sum_{i=1,2}(\mu_{Siz})^2 - H_x\sum_{i=1,2}(\mu_{Lix}+\mu_{Six}) + \sum_{i,j=1,2}\vec{D}_{\mathrm{DM}ij}\cdot(\vec{\mu}_{Si}\times\vec{\mu}_{Lj})$$

where J_{LS}, J_{LL}, and J_{SS} are the superexchange constants of the $L\&S$, $L\&L$, and $S\&S$ blocks; $D_L\&D_S$ are the magnetic anisotropy constants of $L\&S$ blocks along the z axis ($\|[001]$); H_x is the sum of internal ($H_x^{\rm int}$) and external ($H_x^{\rm ext}$) magnetic fields along the x axis ($\|[120]$); $\vec{D}_{\mathrm{DM}ij}$ is the Dzyaloshinskii-Moriya vector between $\vec{\mu}_{Si}\&\vec{\mu}_{Lj}$. Solving the Landau-Lifshitz-Gilbert equation leads to two $k = 0$ normal modes, i.e., low- and high-lying modes that have antiphase modulation between $\vec{\mu}_{L1}\&\vec{\mu}_{L2}$ and between $\vec{\mu}_{S1}\&\vec{\mu}_{S2}$, all of which precess about their static directions (see Sec. 1 in the Supplemental Material [29] for the detailed calculation).

The mode characteristics calculated in reasonable ranges of the parameters can lead us to identify the mode corresponding to the observed electromagnon. To this end, we first deduce magnetization (M_x) vs $H_x^{\rm ext}$ relation from the Hamiltonian (See Sec. 2 in the Supplemental Material [29] for the detailed calculation), and compared it with the experimental data. We use 5 μ_B per each Fe^{3+}/Co^{2+} site, which is in between the spin moment values of Fe^{3+} (Spin $= 5/2$) and Co^{2+} (Spin $= 3/2$). The antiparallel spin alignment within each block leads to $\mu_L = 35\ \mu_B$ and

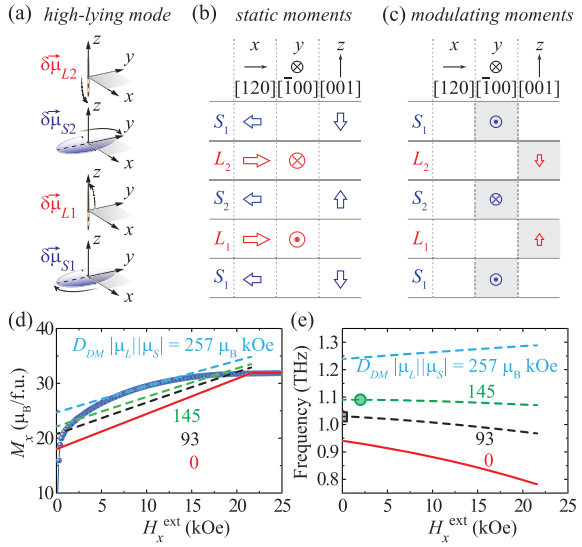

FIG. 4. (a) Trajectories of the high-lying magnon mode. Red (blue) ellipsoid represents the modulation $\delta\vec{\mu}_L(\delta\vec{\mu}_S)$. Summary of x, y, and z components of (b) the static moments and (c) their modulations. (d) Magnetization (M_x) vs external magnetic field $(H_x^{\rm ext})\|[120]$ relations at 20 K. The sphere denotes the experimental data. (e) Calculated frequencies of the high-lying mode under $H_x^{\rm ext}$ for various DM interaction strengths. Solid symbols denote the observed electromagnon resonance frequencies.

$\mu_S = 5\ \mu_B$, respectively. The solid line in Fig. 4(d) is the calculation result based on a set of parameters: $J_{LS}|\mu_L\|\mu_S| = 1783$, $J_{LL}|\mu_L|^2 = 992$, $J_{SS}|\mu_S|^2 = 1174$, $D_S|\mu_S|^2 = -302$, $D_L|\mu_L|^2 = 302$, and $D_{\rm DM}|\mu_L\|\mu_S| = 0\ \mu_B$ kOe. We note that despite long distance between the S blocks, sizable J_{SS} is required to produce the considerable antiparallel components along the z direction between $\vec{\mu}_{S1}\&\vec{\mu}_{S2}$. We postulate that this is a consequence in stacking of many exchange interaction paths along z, of which detail is worthy of further study. The parameters are used to estimate magnon frequencies, and in turn leads to the conclusion that the high-lying mode is consistent with our observation while the low-lying mode has at least 1 order of magnitude lower frequency (see Sec. 2 in the Supplemental Material [29]).

Figure 4(a) illustrates the calculated $\delta\vec{\mu}_L$ and $\delta\vec{\mu}_S$ trajectories of the high-lying mode, which are largely elongated along the z and y axes, respectively. The $\vec{\mu}_{L1}$ and $\vec{\mu}_{S1}$ precess in opposite direction of each other with a phase relation that when $\delta\vec{\mu}_{L1}$ points toward $+z$ direction, $\delta\vec{\mu}_{S1}$ is along the -y direction. Figure 4(c) denotes this modulating relation with the x, y, and z components of $\delta\vec{\mu}_L$ and $\delta\vec{\mu}_S$. We note that this modulation can give rise to the electromagnon via exchange striction. For instance, when $\delta\vec{\mu}_{S1}$ is along the -y direction, it is parallel to the y component of the $\vec{\mu}_{L1}$ while antiparallel to that of $\vec{\mu}_{L2}$ [Figs. 4(b), 4(c)]. The exchange striction leads the S_1 block to repel the L_1 and attract the L_2. In the meantime, $\delta\vec{\mu}_{S2}$ along the $+y$ direction also contributes to this lattice distortion that yields modulating electric polarization (δP) along the z direction. The THz light with $E^{\omega}\|z$ modulates δP, and in turn conversely excites the magnon. This process is consistent with the dynamical ME effect driven by exchange striction already revealed in other multiferroic hexaferrites [5,33].

Confirming the consistent description of the dynamical ME effect, we further move on to uncover the main cause of the observed sensitive magnetochromism by assessing characteristics of the high-lying magnon. We first notice that under the approximation of no DM interaction, the electromagnon resonance frequency monotonically diminishes as the field $H_x^{\rm ext}$ is increased [Fig. 4(e)]. This is indeed inconsistent with the observation of blueshifting at $H_x^{\rm ext} = 2$ kOe and thereby leads to considering the role of the DM interaction. Our calculation shows that the enhanced DM term while the other parameters are fixed in $\mathscr{H}$ results in the elevated frequency vs $H_x^{\rm ext}$ curves with increased slopes as depicted in Fig. 4(e). Thus, the frequency hardening can occur if the DM interaction is increased by $H_x^{\rm ext}$.

The DM interaction has not been considered so far for understanding magnetic properties of hexaferrites. In general, the crystal structures of Y-type and Z-type hexaferrites belong to the $R\bar{3}m$ and $P6_3/mmc$ groups, respectively, of which symmetries cancel out the DM interaction. However, the ME state of the hexaferrites has lowered symmetries associated with $P_{\rm Static}$ and thereby the finite DM interaction can exist. The presence of the DM interaction and its variation under $H_x^{\rm ext}$ is supported by the calculated M_x vs $H_x^{\rm ext}$ lines shown in Fig. 4(d). As the DM interaction is enhanced, the calculated lines are elevated while their slopes become more moderate. The interception of the experimental data with those lines indicates that the DM interaction rises up to ~10 kOe and then diminishes with further increasing $H_x^{\rm ext}$. The microscopic origin of the DM interaction is claimed as the oxygen ion shift responding to $P_{\rm Static}$ by recent synchrotron X-ray diffraction study [34], but the complex crystal structure and ambiguity in the distortion amount has impeded the quantitative calculation by the band theory. Instead, our model that includes the interaction strength $D_{\rm DM}|\mu_L\|\mu_S| = 145\ \mu_B$ kOe ~ 8.1% of the major antiferromagnetic interaction between L and S blocks successfully accounts for the observed electromagnon frequency 1.09 THz at $H_x^{\rm ext} = 2$ kOe [Fig. 4(e)]. The estimated value is reasonably smaller than other magnetic interactions in $\mathscr{H}$ and points to the energy scale of the DM interaction in this Co_2Z-type hexaferrite.

We note the connection between the static ME effect and the DM interaction. The $P_{\rm Static}$ of the Co_2Z-type hexaferrite upon increasing $H_x^{\rm ext}$ initially enhances ($0 < H_x^{\rm ext} < 3$ kOe), diminishes (3 kOe $< H_x^{\rm ext} <$ 21 kOe), and then becomes zero ($H_x^{\rm ext} > 21$ kOe) [26]. As $P_{\rm Static}$ shifts the oxygen ions [34], the DM interaction strength is likely correlated to the variation of $P_{\rm Static}$. Thus, $H_x^{\rm ext} = 2$ kOe may enhance the DM interaction resulting in the increase of the electromagnon frequency. On the other hand, $H\|z$ reduces $P_{\rm Static}$ as the cones of $\vec{\mu}_L\&\vec{\mu}_S$ deviate away from the transverse conical structure and in turn decreases the DM interaction. This interaction change consistently explains

the redshifting at $H_z^{\mathrm{ext}} = 2$ kOe. The sensitive THz magnetochromism of the Co_2Z-type hexaferrite highlights the interconnected nature of the static and dynamical ME effects.

To summarize, the electromagnon in $Ba_{0.5}Sr_{2.5}Co_2Fe_{24}O_{41}$ is observed by THz time-domain spectroscopy. It develops with the transverse conical magnetic order below 410 K and exhibits sensitive magnetochromism at low magnetic fields, both of which have been lacking in multiferroics and thereby serve as unique properties for THz device application. We propose a model Hamiltonian that identifies a magnon mode with an electromagnon resonance in the THz range. The model calculation allows us to uncover that the magnetochromism is the consequence of the Dzyaloshinskii-Moriya interaction, which can be, in turn, modulated by static electric polarization under magnetic fields. This interconnection between the dynamical and static ME effects should be generally present in other multiferroics too and can thus provide a new route to realize THz functionality via the control of electromagnon resonance.

We would like to thank Jong-Woo Kim, Jae-Ho Chung, Hun Jang, and Hak Bong Lee for helpful discussions, and Dae Hoon Han for experimental support. This work was supported by the National Creative Research Initiative (2010-0018300) and Global Collaborative Research Projects (2016K1A4A3914691) through the National Research Foundation (NRF) of Korea. The THz TDS experiment at Seoul National University (2015R1A3A2031768 and 2016R1A3B1908336) and use of the fs-THz beam line at Pohang Light Source (2009-0083512, 2009-0090599) were also supported by the NRF. Work at Argonne National Laboratory was supported by the U.S. Department of Energy (DOE), Office of Science, Basic Energy Sciences, Materials Science and Engineering Division.

*optopia@snu.ac.kr

[1] V. G. Bar'yakhtar and I. E. Chupis, Sov. Phys. Solid State **11**, 2628 (1970).
[2] H. Katsura, A. V. Balatsky, and N. Nagaosa, Phys. Rev. Lett. **98**, 027203 (2007).
[3] A. Pimenov, A. A. Mukhin, V. Yu. Ivanov, V. D. Travkin, A. M. Balbashov, and A. Loidl, Nat. Phys. **2**, 97 (2006).
[4] A. B. Sushkov, R. V. Aguilar, S. Park, S.-W. Cheong, and H. D. Drew, Phys. Rev. Lett. **98**, 027202 (2007).
[5] N. Kida, D. Okuyama, S. Ishiwata, Y. Taguchi, R. Shimano, K. Iwasa, T. Arima, and Y. Tokura, Phys. Rev. B **80**, 220406 (R) (2009); N. Kida, S. Kumakura, S. Ishiwata, Y. Taguchi, and Y. Tokura, Phys. Rev. B **83**, 064422 (2011).
[6] S. Seki, N. Kida, S. Kumakura, R. Shimano, and Y. Tokura, Phys. Rev. Lett. **105**, 097207 (2010).
[7] I. Kézsmárki, N. Kida, H. Murakawa, S. Bordács, Y. Onose, and Y. Tokura, Phys. Rev. Lett. **106**, 057403 (2011).
[8] M. Cazayous, Y. Gallais, A. Sacuto, R. de Sousa, D. Lebeugle, and D. Colson, Phys. Rev. Lett. **101**, 037601 (2008); D. Talbayev, S. A. Trugman, S. Lee, H. T. Yi, S.-W. Cheong, and A. J. Taylor, Phys. Rev. B **83**, 094403 (2011).
[9] S. P. P. Jones, S. M. Gaw, K. I. Doig, D. Prabhakaran, E. M. Hétroy Wheeler, A. T. Boothroyd, and J. Lloyd-Hughes, Nat. Commun. **5**, 3787 (2014).
[10] T. Kimura, T. Goto, H. Shintani, K. Ishizaka, T. Arima, and Y. Tokura, Nature (London) **426**, 55 (2003).
[11] J. Wang, J. B. Neaton, H. Zheng, V. Nagarajan, S. B. Ogale, B. Liu, D. Viehland, V. Vaithyanathan, D. G. Schlom, U. V. Waghmare, N. A. Spaldin, K. M. Rabe, M. Wuttig, and R. Ramesh, Science **299**, 1719 (2003).
[12] N. Hur, S. Park, P. A. Sharma, J. S. Ahn, S. Guha, and S.-W. Cheong, Nature (London) **429**, 392 (2004).
[13] M. Fiebig, J. Phys. D **38**, R123 (2005); W. Eerenstein, N. D. Mathur, and J. F. Scott, Nature (London) **442**, 759 (2006).
[14] D. Senff, P. Link, K. Hradil, A. Hiess, L. P. Regnault, Y. Sidis, N. Aliouane, D. N. Argyriou, and M. Braden, Phys. Rev. Lett. **98**, 137206 (2007).
[15] Y. Takahashi, R. Shimano, Y. Kaneko, H. Murakawa, and Y. Tokura, Nat. Phys. **8**, 121 (2012).
[16] T. Kubacka, J. A. Johnson, M. C. Hoffmann, C. Vicario, S. de Jong, P. Beaud, S. Grübel, S.-W. Huang, L. Huber, L. Patthey, Y.-D. Chuang, J. J. Turner, G. L. Dakovski, W.-S. Lee, M. P. Minitti, W. Schlotter, R. G. Moore, C. P. Hauri, S. M. Koohpayeh, V. Scagnoli, G. Ingold, S. L. Johnson, and U. Staub, Science **343**, 1333 (2014).
[17] H. Katsura, N. Nagaosa, and A. V. Balatsky, Phys. Rev. Lett. **95**, 057205 (2005); M. Mostovoy, Phys. Rev. Lett. **96**, 067601 (2006); I. A. Sergienko and E. Dagotto, Phys. Rev. B **73**, 094434 (2006).
[18] L. C. Chapon, G. R. Blake, M. J. Gutmann, S. Park, N. Hur, P. G. Radaelli, and S.-W. Cheong, Phys. Rev. Lett. **93**, 177402 (2004).
[19] C. Jia, S. Onoda, N. Nagaosa, and J. H. Han, Phys. Rev. B **76**, 144424 (2007); T. Arima, J. Phys. Soc. Jpn. **76**, 073702 (2007).
[20] R. Valdes Aguilar, M. Mostovoy, A. B. Sushkov, C. L. Zhang, Y. J. Choi, S.-W. Cheong, and H. D. Drew, Phys. Rev. Lett. **102**, 047203 (2009).
[21] N. Kida, Y. Takahashi, J. S. Lee, R. Shimano, Y. Yamasaki, Y. Kaneko, S. Miyahara, N. Furukawa, T. Arima, and Y. Tokura, J. Opt. Soc. Am. B **26**, A35 (2009).
[22] M. Mochizuki, N. Furukawa, and N. Nagaosa, Phys. Rev. Lett. **104**, 177206 (2010).
[23] M. Tonouchi, Nat. Photonics **1**, 97 (2007).
[24] Y. Kitagawa, Y. Hiraoka, T. Honda, T. Ishikura, H. Nakamura, and T. Kimura, Nat. Mater. **9**, 797 (2010).
[25] M. Soda, T. Ishikura, H. Nakamura, Y. Wakabayashi, and T. Kimura, Phys. Rev. Lett. **106**, 087201 (2011).
[26] S. H. Chun, Y. S. Chai, B.-G. Jeon, H. J. Kim, Y. S. Oh, I. Kim, H. Kim, B. J. Jeon, S. Y. Haam, J.-Y. Park, S. H. Lee, J.-H. Chung, J.-H. Park, and K. H. Kim, Phys. Rev. Lett. **108**, 177201 (2012).
[27] F. Kadlec, C. Kadlec, J. Vít, F. Borodavka, M. Kempa, J. Prokleška, Josef Buršík, R. Uhrecký, S. Rols, Y. S. Chai, K. Zhai, Y. Sun, J. Drahokoupil, V. Goian, and S. Kamba, Phys. Rev. B **94**, 024419 (2016).
[28] D. Talbayev, S. A. Trugman, A. V. Balatsky, T. Kimura, A. J. Taylor, and R. D. Averitt, Phys. Rev. Lett. **101**, 097603 (2008).

[29] See Supplemental Material at http://link.aps.org/supplemental/10.1103/PhysRevLett.120.027202 for the calculation of magnon frequency and the extraction of parameters in H from the relation of magnetization, which includes Refs. [26,28,30–32].

[30] H. B. Lee, Y.-S. Song, J.-H. Chung, S. H. Chun, Y. S. Chai, K. H. Kim, M. Reehuis, K. Prokeš, and S. Mat'aš, Phys. Rev. B **83**, 144425 (2011).

[31] H. B. Lee, S. H. Chun, K. W. Shin, B.-G. Jeon, Y. S. Chai, K. H. Kim, J. Schefer, H. Chang, S.-N. Yun, T.-Y. Joung, and J.-H. Chung, Phys. Rev. B **86**, 094435 (2012).

[32] J. Smit and H. P. J. Wijn, *Ferrites* (Phillips Technical Library, Eindhoven, Netherlands, 1959).

[33] T. Nakajima, Y. Tokunaga, M. Matsuda, S. Dissanayake, J. Fernandez-Baca, K. Kakurai, Y. Taguchi, Y. Tokura, and T. Arima, Phys. Rev. B **94**, 195154 (2016).

[34] S. H. Chun, K. W. Shin, K. H. Kim, J. F. Mitchell, P. J. Ryan, and J.-W. Kim, arXiv:1706.01144.